World Academy of Science, Engineering and Technology
International Journal of Aerospace and Mechanical Engineering
Vol:6, No:8, 2012

Comparative Evaluation of Ice Adhesion Behavior

T. Strobl, D. Raps, M. Hornung

***Abstract*—In this study, the adhesion of ice to solid substrates with different surface properties is compared. Clear ice, similar to atmospheric in-flight icing encounters, is accreted on the different substrates under controlled conditions. The ice adhesion behavior is investigated by means of a dynamic vibration testing technique with an electromagnetic shaker initiating ice de-bonding in the interface between the substrate and the ice. The results of the experiments reveal that the affinity for ice accretion is significantly influenced by the water contact angle of the respective sample.

***Keywords*—Contact angle, dynamic vibration measurement, ice adhesion, interfacial shear stress.

I. INTRODUCTION

THE adhesion and deposition of ice adversely affects many fields of civilization. With respect to aviation, the formation of ice on main aircraft structural components degrades the aerodynamic efficiency of the airfoil and the aircraft, respectively [1]–[3]. In a worst case scenario, ice accretion might eventually cause such problems that control of the airplane is completely lost [4]. The way of counteracting ice contamination can be carried out by either removing ice deposits through active aircraft de-icing systems on the basis of electro-mechanical, chemical and thermal principles, or by means of beneficial coatings that prevent the ice to stick to the surfaces.

Even though there is no solid material that can entirely prevent ice from adhering to its surface, this study aims at the examination of the ice adhesion phenomenon based upon the principle of harmonic excitation. Through the use of a dynamic vibration measurement technique with an electro-magnetic shaker, which is seen as a viable testing method, the interfacial forces between ice and various materials are characterized [5]–[7]. The identification of the influence of surface coatings and the extent to which ice phobic coatings are able to delay or almost avoid ice formation on aircraft surfaces are the primary objectives of the underlying study.

T. Strobl is with the EADS Innovation Works, Metallic Technologies and Surface Engineering, EADS Deutschland GmbH, 81663 Munich, Germany (phone: +49 89 607 20748; e-mail: Tobias.Strobl@eads.net).

D. Raps is with the EADS Innovation Works, Metallic Technologies and Surface Engineering, EADS Deutschland GmbH, 81663 Munich, Germany (e-mail: Dominik.Raps@eads.net).

M. Hornung is with the Institute of Aircraft Design, Technical University of Munich, Boltzmannstraße 15, 85748 Garching, Germany (e-mail: Mirko.Hornung@tum.de).

II. ANALYTICAL COMPUTATIONS

A. Euler-Bernoulli Beam Theory

The displacement and resultant internal stresses due to the application of an external load to an originally undeformed cantilever beam with a homogeneous cross section can be determined by means of the classical beam theory of Euler and Bernoulli according to the fourth order differential equation:

$$EI_y \frac{d^4 w(x)}{dx^4} = q \tag{1}$$

where E is the Young's modulus of the material, I_y denotes the second moment of area of the cross section about the lateral axis (y-axis), $w(x)$ is the deflection of the beam at the position x along the longitudinal axis (x-axis) and q is a distributed load [8]. It is worth mentioning that (1) underlies several assumptions as given in [8].

Within the scope of this research, the deformation and the resultant internal stresses are referred to an ice-aluminum composite beam. For the purpose of illustration, the bending deflection and the corresponding internal normal and shear stresses σ and τ for the ice-aluminum composite beam are depicted (see Figure 1). Adhesive failure at the interface between the ice and the aluminum substrate is primarily caused by shear stresses [5], [9]. According to Figure 1, the maximum magnitude of the shear stress τ_{max} is obtained at the position of the neutral axis (N.A.) of the ice-aluminum cross section. Hence, the thickness of the ice layer h_{ice} has to be chosen in such a way that the neutral axis of the ice-aluminum composite beam coincides with the interface between the ice and the aluminum. However, due to limitations in the experimental set-up, the neutral axis of the ice-substrate composite beams can only be positioned in the vicinity of the ice-aluminum interface and not exactly in the interface.

The computation of the shear stresses in composite beams is carried out in the same way as ordinary shear stress determination for homogeneous cross sections [10]. The corresponding equation for the shear stress τ at the respective vertical position $\bar{z}$ of the composite beam is:

$$\tau(\bar{z}) = \frac{Q\,\overline{ES_y(\bar{z})}}{\overline{EI}\,b(\bar{z})} \tag{2}$$

where Q is the transverse shear force, S_y is the first moment of area with respect to the vertical axis (z-axis) and b is the beam width. Note that the accent mark $\bar{}$ is meant to illustrate that the respective parameter refers to the equivalent $\bar{y}$-$\bar{z}$ coordinate system (see Figure 1). Substituting the respective

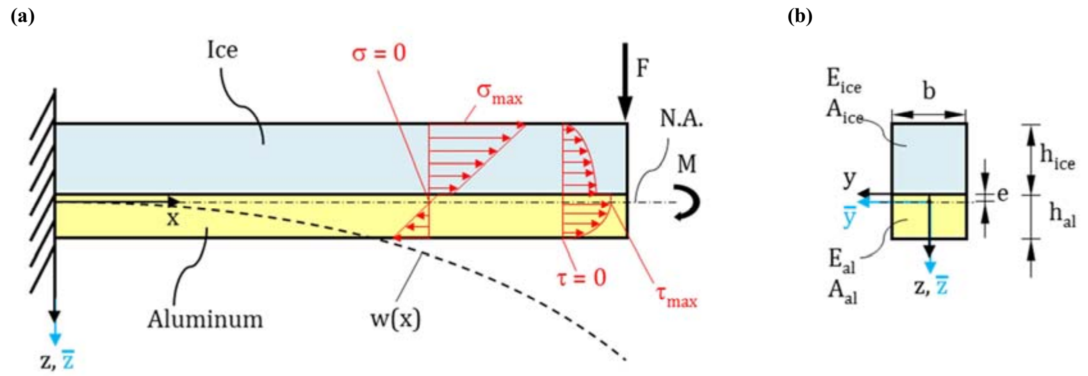

Fig. 1 (a) Lateral view of the ice-aluminum composite beam and resultant internal normal stresses $\boldsymbol{\sigma}$ and shear stresses $\boldsymbol{\tau}$ due to external load application *F*. (b) Cross section of the ice-aluminum composite beam

parameters into (2) as given in [8] and rearranging (2) finally yields the interfacial shear stress τ_{int} of the ice-aluminum composite beam:

$$\tau_{int} = \frac{\varepsilon_{EF\_al}\, E_{ice}\left(h_{ice}{}^{2} + 2h_{ice}|e|\right)}{2\,(x-l)\,(h_{al}-|e|)} \tag{3}$$

where ε_{EF_al} indicates the strain at the extreme fiber at the bottom of the aluminum layer, which is measured experimentally by strain gauges. In this context, x is the distance between the center of the strain gauges and the clamped end of the beam (see Figure 1). Additionally, l is the total length of the composite beam, h is the thickness of the ice and respectively of the aluminum layer, and e is the excentricity [8]. Note that the shear stress computation refers to the vertical position $\bar{z} = |e|$, which is close to the interface between the aluminum and the ice.

B. Dynamic Beam Excitation

The dynamic response of a cantilever beam due to a sinusoidal stimulus can be determined by the differential equation of motion of an Euler-Bernoulli beam for dynamic bending:

$$\frac{EI_y}{\rho A}\frac{d^4 w(x,t)}{dx^4} + \frac{d^2 w(x,t)}{dt^2} = 0 \tag{4}$$

where E is the Young's modulus of the material, ρ is the density, I_y denotes the second moment of area of the cross section about the y-axis, A is the cross sectional area of the beam and $w(x,t)$ is the bending displacement at the position x at the time t [11]. The maximum dynamic bending stress that can be applied to the beam is obtained at its first resonance frequency [7]. The corresponding formula for the first resonance frequency of the cantilever beam can be written as:

$$f_1 \approx 0.560\sqrt{\frac{EI_y}{\rho A l_{osc}{}^{4}}} \tag{5}$$

where l_{osc} is the free oscillating length of the beam [11].

III. Experimental Procedures

A number of laboratory experiments were conducted in the past to study the adhesive properties of ice on solid surfaces [5]–[7], [12]. However, within these previous studies, the ice was frozen on the metal substrates in a non-supercooled state. As covered by this research, the water is frozen onto the specimens by means of a spraying procedure which is comparable to the process of atmospheric ice accretion on aircraft structures. Within the experimental procedure, the ice is considered as polycrystalline ice I_h, which generally is formed when liquid water is cooled down below zero degrees Celsius (°C) at standard atmospheric pressure (1.01325 bar) [13]. The density ρ of ice I_h at 0 °C is equal to 0.91671 ± 0.00005 g/cm³ and the Young's modulus of ice roughly amounts to 9.0 GPa [9], [14]. In addition, the Poisson ratio of isotropic polycrystalline ice was determined as to be 0.325 [15]. Table I. summarizes the main physical parameters for polycrystalline ice I_h.

A. Experimental Set-Up

The experimental set-up for the ice adhesion tests consists of the equipment for ice preparation and the test bench for the dynamic vibration measurements. All the sample preparations and experimental investigations are carried out within a top-opening chest freezer at temperatures in the range between -14.0 and -16.0 °C. Four different substrates, namely the aluminum alloy AA 2024 reference specimen, an anodized AA 2024 sample, an AA 2024 substrate with a hard anodizing layer that contains embedded particles of Teflon (PTFE) and a sample with a hydrophobic coating, are tested. The aim is to show that the degree of ice adhesion can be reduced by the use of functional and respectively icephobic coatings. For this purpose, the water contact angle θ of the different substrates is

TABLE I
Main Parameters for Polycrystalline Ice I_h

Symbol	Parameter	Value
ρ	Density	0.91671 ± 0.00005 g/cm³ [14]
E	Young's modulus	9.0 GPa [9]
ν	Poisson ratio	0.325 [15]

measured prior to ice accretion through the use of a Krüss contact angle measuring system G10 equipped with a 6.4 mm x 4.8 mm CCD Camera. Subsequently, the samples are placed into a PVC mold at one side to provide an ice-free area on the substrate surface for the subsequent clamping to the electro-magnetic shaker. The accretion of a constant layer of clear ice on the substrates is achieved by spraying water with a defined droplet size through the use of an ultrasonic atomizer of type US1 T710.070.16.50 provided by the Lechler GmbH (see [16], [17]). For the purpose of repeatability and to achieve experimental results being comparable to atmospheric in-flight icing encounters, the water used within the experimental investigations is deionized water with an electrical conductivity of 6.0 x 10^{-4} $S{\cdot}m^{-1}$. Additionally, the water is pre-cooled to a target temperature in the range between +0.4 °C and +0.8 °C by means of a ThermoHaake thermostat of type P1-40P.

The dynamic vibration test bench mainly consists of a vibration test system, comprising an electro-magnetic shaker of Ling Dynamic Systems (LDS) and a Kontron-type power amplifier. Additionally, a process computer and a Hottinger Baldwin Messtechnik (HBM) measuring amplifier system are used for data acquisition, including HBM strain gauges that are bonded to the metal samples. The experimental set-up of the dynamic vibration technique is schematically illustrated in Figure 2.

B. Measurement Procedure

Providing a thickness of 1.60 mm, the coated and uncoated metal samples are trimmed by a milling cutter to a width of 17.00 mm and a length of 80.00 mm (see Figure 3). In a similar manner to [6], one strain gauge is attached to each specimen at 10.00 mm from the end where the ice-substrate composite beams are subsequently clamped onto the electro-magnetic shaker (see Figures 3, 4a and 4b). Note that the strain gauges are bonded to the bottom side of the ice-aluminum composite beams, which is not covered by water and respectively ice in the subsequent procedure. The upper surface of the specimens is then carefully cleaned with an isopropyl alcohol solution and dried with compressed air.

Prior to ice accretion, the contact angle θ of each substrate is measured with water. Each sample is measured at three different points and 30 measurements are carried out per point. The contact angle is calculated as mean value from these measurements. The specimens are then clamped onto the PVC mold and kept in the chest freezer to cool down the surface temperature of the samples to approximately -16 °C. Super-

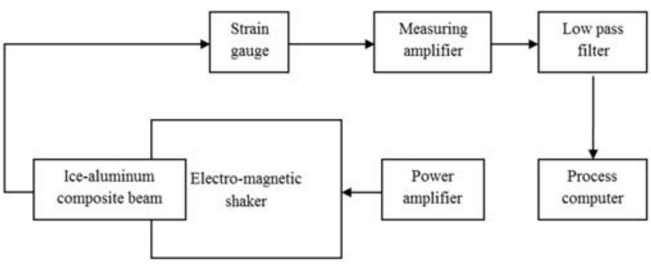

Fig. 2 Schematic experimental set-up of the dynamic vibration test rig

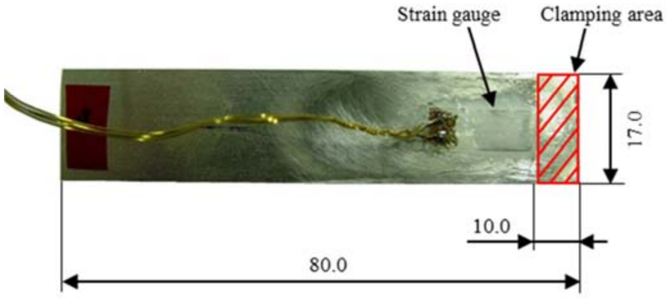

Fig. 3 Strain gauge bonded to the un-iced side of a sample specimen

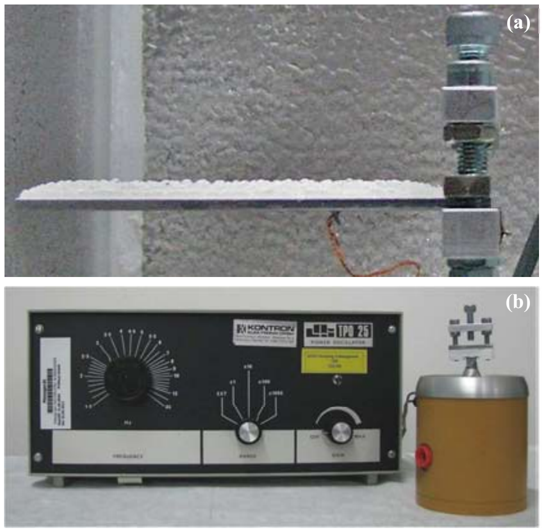

Fig. 4 (a) Lateral view of the clamped ice-aluminum composite beam and (b) Electro-magnetic shaker system

cooled water droplets with an average droplet diameter of 20 microns are deposited on the pre-cooled specimens by means of the ultrasonic atomizer for the duration of 15 minutes. In addition, the atomizer is cooled down by means of liquid-nitrogen to prevent re-warming of the water droplets and to generate circular atomization of the fine spray of water droplets. The free-falling water droplets, still remaining in liquid state, impinge on the surface of the substrates and freeze onto these top surfaces as an appropriate film of clear ice. The ice-substrate composite beams are then carefully removed out of the PVC mold and lateral photographs are taken of the specimens for the determination of the ice thickness h_{ice}. For each sample, the ice thickness is measured at ten different reference points and the respective average value is calculated.

Subsequent to the ice accretion process, each ice-substrate composite beam is centrically clamped onto the electro-magnetic shaker, which is illustrated in Figure 4a. The shaker was loaded in the chest freezer before to provide an environment with constant sub-zero temperatures for the experiments. Each ice-substrate composite beam is vibrated by means of the electro-magnetic shaker submitting a sinusoidal stimulus to the sample. The excitation frequency for the harmonic oscillation is analytically determined by means of (5). Since the ice layer is not continuously accreted on the substrate surface over the entire length and due to the damping effect of the strain gauge as well, the first resonance frequency of the ice-substrate composite beam is approached through the determination of the first resonance frequency of the bare aluminum beam without ice coating and strain gauge. The material characteristics of the aluminum beam used for the computation are presented in Table II. Taking into consideration the given parameters and dimensions, the first resonance frequency of the aluminum beam without ice coating is equal to approximately 254.0 Hz. The excitation amplitude of the shaker is then increased until the resultant interfacial shear stress leads to ice de-bonding from the substrate surface, i.e. adhesive failure occurs in the interface between the ice and the metal substrate.

By means of the strain gauge reading, the adhesive failure can be detected as the bending stiffness of the composite beam changes due to ice breakage and subsequent delamination from the beam surface. Figure 5 illustrates an exemplary strain gauge reading of an ice-substrate composite beam under harmonic excitation, where 500 reading points are recorded every second. The delamination process of the ice from the sample can be subdivided into three phases. The first phase is characterized by a continuous increase in the oscillation amplitude, ending with a sudden peak in the vertical axis of the vibration pattern. This is the point where the ice starts to de-bond from the substrate surface. As visually observed, the ice starts to delaminate close to the clamping of the composite beam due to the fact that within this area, the maximum bending moment along the x-axis is obtained. After the initiation of ice delamination, the amplitude is not increased further. The second phase of the waveform of the oscillatory motion is characterized by a maximum in the oscillation amplitude, which is caused by the instantaneous decrease in the bending stiffness of the beam due to the ice delamination. Hence, the damping effect of the ice on the vibrational motion is reduced and the oscillatory motion requires a certain time to settle down at a stable level. Since the excitation amplitude is constant in the ensuing period, the third phase shows constant values for the strain of the beam. Within this phase, the measurement reading of Figure 5 shows considerably higher values for the strain as the excitation frequency of the beam with (partially) de-bonded ice layer was close to its first resonance frequency. For the determination of the maximum adhesion strength of ice onto solid surfaces, the corresponding reading of the strain gauge is considered on the verge of the sudden peak at the end of phase one, where the ice layer is still entirely bonded to the metal substrate. This value of the strain ε_{EF_al} is substituted into (3) to compute the maximum admissible shear stress τ_{int} at the interface between the ice and the aluminum beam just before the ice detaches.

TABLE II
MATERIAL CHARACTERISTICS AND DIMENSIONS OF THE ALUMINUM BEAM

Symbol	Parameter	Value
ρ	Density	2.7 g/cm³
E	Young's modulus	70.0 GPa
A	Cross-sectional area	27.2 mm²
I_y	Second moment of area	5.8 mm⁴
l_{osc}	Free oscillating length	72.0 mm

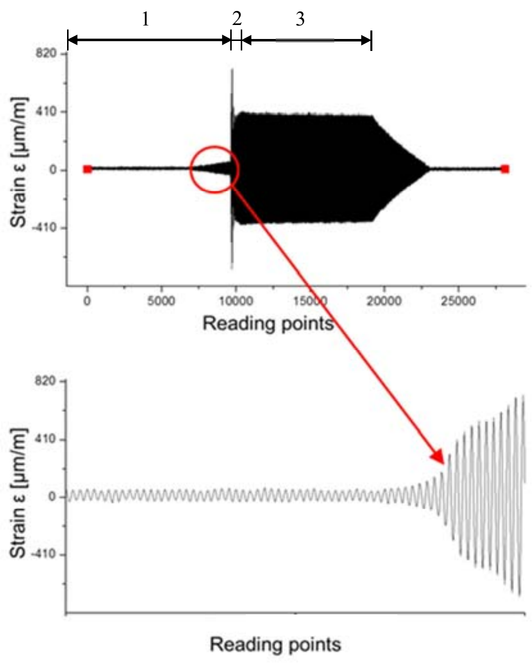

Fig. 5 Strain gauge reading of an ice-substrate composite beam

IV. RESULTS AND DISCUSSION

Prior to the ice adhesion tests with the dynamic measurement technique, the contact angle θ with water is determined for each substrate. The results of the contact angle measurements are illustrated in Figure 6. The AA 2024 clad sample is referred to as a reference material within the scope of this research. The water contact angle can be considered as rather low with a magnitude of 65.3 ± 6 °, which is mainly caused by the presence of hydroxyl groups at the substrate surface of the AA 2024 reference specimen. The anodized AA 2024 sample is obtained by anodizing of the reference test specimen in tartaric sulphuric acid (TSA) solution after acidic pickling, followed by a final rinse. The outcome is a hydrophilic aluminum oxide layer with a coating thickness of approximately 3 µm. In particular, the anodization causes an

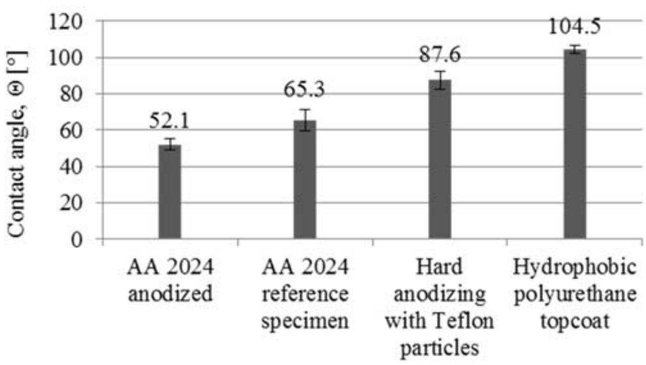

Fig. 6 Measurement of the contact angle θ with water of the substrates

increased amount of hydrophilic OH^--groups upon the surface of the sample while simultaneously enhancing the surface area of the substrate, i.e. there are more open pores at the surface. Hence, the anodized AA 2024 specimen has a very low water contact angle with a magnitude of 52.1 ± 3 °, which means a high degree of water-wetting on the surface. In accordance with [18], Teflon generally has a considerable positive effect on the hydrophobicity of a surface, i.e. the contact angle with water of the respective surface is increased to a large extent. This equally applies to the hard anodizing coating with embedded Teflon particles in a slightly reduced manner, where the contact angle with water is measured to be equal to 87.6 ± 5 °. The hydrophobic polyurethane coating is characterized by a high content of functional groups.

Since these functional groups are present on the outermost layer of the sample the surface energy of the coating is reduced to a large extent. Hence, the interfacial forces of attraction between the water molecules and the substrate surface are low, which leads to a large water contact angle with a magnitude of 104.5 ± 2 °.

For the evaluation of the degree of ice adherence to the four different substrates, a series of three measurements is performed on the dynamic vibration test rig. Figure 7 shows the mean values of the maximum interfacial shear stress τ_{int} plotted against the water contact angle θ of the respective substrate surface. The lowest value of interfacial shear stress is obtained for the hydrophobic polyurethane coating with a magnitude of 0.025 ± 0.008 MPa. The reason for the very low adhesion of ice to this coating is based upon the large contact angle with water. This means that solely a small part of each individual water droplet is in intimate contact with the substrate surface and respectively freezes onto it. Thus, the ice accreted on this hydrophobic coating is easy to remove. The measurement results also indicate that the presence of embedded Teflon (PTFE) particles in the hard anodizing layer leads to a rather low value of ice adhesion with a magnitude of 0.044 ± 0.005 MPa. However, since the coating contains Teflon particles to a limited extent, its contact angle with water does not attain typical values for Teflon such as 108° as stated by Ref. [18]. Hence, the efforts to remove the ice from this coating are in excess of those applying to coatings that are entirely made out of Teflon. Comparing the AA 2024 clad reference sample to the previous coatings the adhesion of ice to the former increases up to a magnitude of 0.050 ± 0.005 MPa. This is due to the presence of hydroxyl groups at the substrate surface and the resultant increase in the degree of hydrophility, which is depicted by the decrease in the water contact angle. The anodized AA 2024 sample shows the highest value of ice adhesion to the substrate material in the experiments. In accordance with Ref. [19], reactive groups with available bonding sites such as the OH^--groups on the surface of the anodized sample considerably increase the attraction between the ice and the substrate surface. Thus, the ice adhesion behavior of the anodized AA 2024 specimen is related to the large amount of hydrophilic OH^--groups and also to the open porous aluminum oxide surface structure. Taken together, this leads to a high mean value of the interfacial shear stress τ_{int} with a magnitude of 0.072 ± 0.006 MPa.

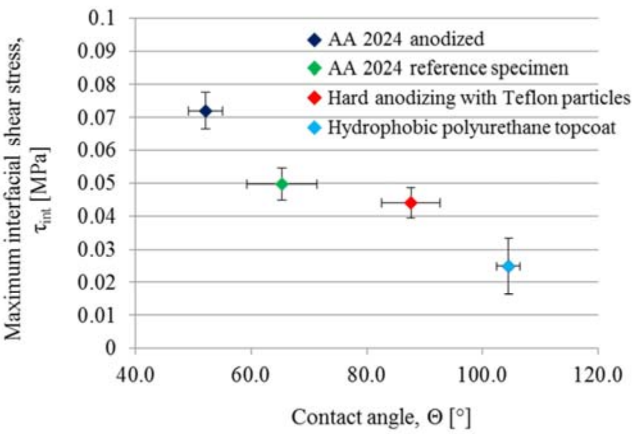

Fig. 7 Relation between the water contact angle θ and the maximum interfacial shear stress τ_{int} of the ice-substrate composite beams

V. Summary

Within this study, the interfacial shear stress τ_{int} between ice and different substrates was investigated in relation to the degree of water-wetting and respectively the hydrophobicity. The main conclusion is that very high contact angles are good for low ice adhesion properties. In this context, hydrophobic coatings with a contact angle θ greater than 90 ° showed the best performance with respect to their affinity to stick to ice. For future aircraft applications, it will be of great interest to further investigate the optimum surface roughness combined with a very high water contact angle for ease in ice removal.

Acknowledgment

The authors gratefully acknowledge the suggestions and academic assistance of Daniel Paulus, PhD student at the Institute of Aircraft Design at the Technical University of Munich.

References

[1] Aviatas. (2011). Stall Angles (Ice). Retrieved May 16, 2011, from http://www.aviatas.com/worksamples/ice_stall.php.

[2] Civil Aviation Authority. (2000, June 14). Aircraft Icing Handbook. Retrieved April 09, 2011, from http://www.caa.govt.nz/search/query.asp.

[3] Federal Aviation Administration. (2007, December 31). Advisory Circular AC 91-74A - Pilot Guide: Flight in Icing Conditions. Retrieved April 09, 2011, from http://rgl.faa.gov/REGULATORY_AND_GUIDANCE_LIBRARY%5CRGADVISORYCIRCULAR.NSF/0/4C8192BB0B733862862573D2005E7151?OpenDocument.

[4] AOPA-Germany. (2001, January). *AOPA-Letter 1/ 2001 - Flugzeugvereisung.* Retrieved April 09, 2011, from www.aopa.de/DE/upload/pdf/PDFLetter/2001-Letter_1/Letter_1-2001-16-18%2B38.pdf.

[5] Akitegetse, C., Volat, C., & Farzaneh, M. (2008). Measuring bending stress on an ice/aluminium composite beam interface using an embedded piezoelectric PVDF (polyvinylidene-fluoride) film sensor. Meas. Sci. Technol. (19), 1-9.

[6] Hassan, M. F., Lee, H. P., & Lim, S. P. (2010). The variation of ice adhesion strength with substrate surface roughness. Meas. Sci. Technol. (21), 1-9.

[7] Javan-Mashmool, M., Volat, C., & Farzaneh, M. (2006). A new method for measuring ice adhesion strength at an ice–substrate interface. *Hydrol. Process.* (20), 645–655.

[8] Gross, D., Hauger, W., Schnell, W., & Schröder, J. (2005). *Technische Mechanik 2 Elastostatik* (Vol. 2). Darmstadt und Essen: Springer Verlag.

[9] Mojtaba, E. (2005). *Ice shedding from overhead electrical lines by mechanical breaking: a ductile model for viscoplastic behaviour of atmospheric ice.* Chicoutimi: Université du Québec.

[10] Wriggers, P., Nackenhorst, U., Beuermann, S., Spiess, H., & Löhnert, S. (2006). *Technische Mechanik kompakt Starrkörperstatik Elastostatik Kinetik* (2. Auflage ed.). Wiesbaden: Teubner.

[11] Ganci, S. (2009). A simple experiment on flexural vibrations and Young's modulus measurement. *Physics Education , 44* (3), 236-240.

[12] Archer, P., & Gupta, V. (1998). Measurement and control of ice adhesion to aluminum 6061 alloy. *J. Mech. Phys. Solids* (46), 1745-71.

[13] Hobbs, P. V. (1974). *Ice Physics.* London: Oxford University Press.

[14] Ginnings, D. C., & Corruccini, R. J. (1947). An improved ice calorimeter - the determination of its calibration factor and the density of ice at 0°C. *J. Res. natn Bur. Stand* (38), 583-91.

[15] Gammon, P. H., Kiefte, H., Clouter, M. J., & Denner, W. W. (1983). Elastic Constants of Artificial and Natural Ice Samples by Brillouin Spectroscopy. *Journal of Glaciology , 29* (103), 433-60.

[16] Lechler GmbH. (1995). *Operation Instruction Ultrasonic atomizer US 1.* Precision Nozzles; Nozzle Systems. Metzingen / Germany: Lechler GmbH.

[17] Lechler GmbH. (2008). *Ultrasonic atomizer.* Precision Nozzles; Nozzle Systems. Metzingen / Germany: Lechler GmbH.

[18] Raraty, L. E., & Tabor, D. (1958). The adhesion and strength properties of ice. *Proc. R. Soc.* (A 245), 184-201.

[19] Sivas, S. L., Riegler, B., Thomaier, R., & Hoover, K. (2004). *A Silicone-Based Ice Phobic Coating for Aircraft.* The Department of the Army, Engineer Research and Development Center, Cold Regions Research and Engineering Laboratory (CRREL). Hanover, NH, U.S.: Pratt & Whitney.